Weak, Seismogenic Faults Inherited From Mesozoic Rifts Control Mountain Building in the Andean Foreland

Sam Wimpenny[1*]

[1]COMET, Bullard Laboratories, Department of Earth Sciences,

University of Cambridge, UK

*email: *sew57@cam.ac.uk*

Key Points:

- Weak faults inherited from Mesozoic rifts in the forelands of the northern and southern Andes break the entire crust to 30–45 km depth.
- In the central Andean plateau, the rifts are internal to the mountain range, and the forelands are underthrusting beneath the plateau.
- The mechanisms that can account for frictionally-weak faults in the dry, granulitic lower crust remain unclear.

Key Words:

- 7230 Seismicity and Tectonics
- 8102 Continental orogenic belts and inversion tectonics
- 8163 Rheology and friction of fault zones
- 8004 Dynamics and mechanics of faulting
- 8045 Role of fluids

This paper is a pre-print, therefore has not been through peer review and is currently being considered for publication in Geophysics, Geochemistry, Geosystems.

Abstract

New earthquake focal mechanism and centroid depth estimates show that the deformation style in the forelands of the Andes is spatially correlated with rift systems that stretched the South American lithosphere in the Mesozoic. Where the rifts trend sub-parallel to the Andean range front, normal faults inherited from the rifts are being reactivated as reverse faults, causing the 30–45 km thick seismogenic layer to break up. Where the rift systems are absent from beneath the range front, the seismogenic layer is bending and being thrust beneath the Andes like a rigid plate. Force-balance calculations show that the faults inerhited from former rift zones have an effective coefficient of static friction $\mu' < 0.2$. In order for these frictionally-weak faults to remain seismogenic in the lower crust, their wall rocks are likely to be formed of dry granulite. Xenolith data support this view, and suggest that parts of the lower crust are now mostly metastable, having experienced temperatures at least 75–250 $^{\circ}C$ hotter than present. The conditions in the lower crust make it unlikely that highly-pressurised free water, or networks of intrinsically-weak phyllosilicate minerals, are the cause of their low effective friction, as, at such high temperatures, both mechanisms would cause the faults to deform through viscous creep and not frictional slip. Therefore pre-existing faults in the Andean forelands have remained weak and seismogenic after reactivation, and have influenced the style of mountain building in South America. However, the controls on their mechanical properties in the lower crust remain unclear.

Plain Language Summary

Some mountain belts are narrow and linear in map view, whilst others are wide and curved. The Andes are unique in that they are linear in some parts, but curved in others. In this study, I show that the distribution and types of earthquakes along the margins of the Andes vary systematically with the shape of the mountain belt. Where the mountains are linear, the rocks along the edge of the mountain belt are breaking in earthquakes along pre-existing, frictionally-weak faults. Where the mountains are curved, the rocks along the edge of the mountain belt do not contain any weak faults and they are being thrust beneath the Andes like a rigid plate. Therefore, the properties of faults in the rocks along the margins of the Andes have controlled the shape and evolution of the mountain belt. Notably, the earthquake-generating faults are much weaker than predicted by laboratory experiments. No existing theory can account for the weakness of these seismogenic faults in the extremely dry, strong lower crust.

1 Introduction

The frictional properties of faults in the forelands of mountain ranges play a key role in controlling the style and location of mountain building [Jackson, 2002; Butler et al., 2006]. Where faults are too strong to rupture in response to the forces acting through the lithosphere, the foreland may behave as a rigid plate and be thrust beneath the mountain range below a shallowly-dipping décollement. In contrast, where faults are weak enough to rupture in response to the forces acting through the lithosphere, the foreland may break up, creating a region of distributed shortening and intense seismicity. These contrasting styles of mountain building have been recognised along the eastern margin of the Andes mountains [Jordan et al., 1983; Kley et al., 1999], making the Andean forelands a unique environment to study fault mechanics and its influence on the structure and evolution of mountain ranges.

Our understanding of fault friction remains rooted in the results of laboratory experiments. Lab measurements of the static coefficient of friction (μ) for most rock types are consistently between 0.6 and 0.85, a widely-applied result known as 'Byerlee's Law' [Byerlee, 1978]. However, *in-situ* estimates of the effective coefficient of static friction (μ') on seismogenic faults are between 0.05 and 0.3 [Copley, 2018]. The differences between the laboratory and *in-situ* estimates of static friction have been accounted for by invoking either: (1) highly-pressurised pore fluids, often assumed to be water, that reduce the effective stresses within the cores of active faults [Hubbert and Rubey, 1959], or (2) networks of intrinsically-weak phyllosilicates produced through water-mediated alteration of the rocks in the cores of active faults [Imber et al., 1997]. Geological evidence of both transiently-high fluid pressures and phyllosilicate-rich lithologies is widespread within ancient continental fault zones exhumed from depths of less than 20 km, indicating that water-assisted processes may be critical to generating frictionally-weak faults in the upper crust [e.g. Sibson, 1990; Collettini et al., 2019].

Despite the consensus regarding the geological controls on fault mechanics in the upper crust, the mechanics of seismogenic faults in the lower crust remain enigmatic. For example, along the margins of the Andes mountains in central Peru, seismogenic faults cutting through the ∼40 km thick foreland crust have been shown to have a low effective coefficient of friction compared to Byerlee's Law [Wimpenny et al., 2018]. Unlike most continental fault zones, which only generate earthquakes in the upper 10–20 km of the crust, these faults in central Peru remain seismogenic into the lower crust. Because the faults remain seismogenic at such high pressures and temperatures, the lower crust that surrounds them is thought to be formed of a load-bearing network of anhydrous minerals that contains little or no free pore water [Yardley and Valley, 1997; Jackson et al., 2004]. Solid-state creep rates in the

anhydrous mineral network will be highly sensitive to even trace amounts of inter- and intra-crystalline water ingress [Bürgmann and Dresen, 2008], and the stable hydrous mineral assemblages that form in the lower crust will be different to those present within the shallow crust [e.g. Andersen et al., 1991]. As a result, there is reason to question whether the same water-assisted mechanisms that have been invoked to account for weak faults in the upper crust are also applicable to these seismogenic, lower-crustal fault zones. Vast areas of anhydrous rocks regularly form the forelands of the highest mountain ranges on Earth [Jackson et al., 2021; Weller et al., 2021]. Therefore, developing an understanding of the mechanics of fault zones within the anhydrous lower crust, like those in central Peru, is key to constructing physical models of the growth and evolution of mountain ranges.

In this study, I determine the mechanical properties and geological history of the fault zones along the eastern margins of the Andes, and explore how these faults influence the distribution and style of mountain building. I begin by using new estimates of the focal mechanisms and centroid depths of earthquakes to map out variations in the style of crustal shortening throughout the Andean forelands. I then compare the pattern of seismicity with the location of pre-existing faults in the South American foreland lithosphere. I place bounds on the frictional properties of the seismogenic faults within the Andean forelands using force-balance calculations, and use published xenolith thermobarometry and thermo-kinematic modelling to constrain the geological conditions in the lower crust through which the seismogenic faults cut. Finally, I discuss the implications of these findings for structural inheritance and the evolution of mountain ranges, and the mechanisms that may account for the frictional properties of faults within the anhydrous lower crust.

2 Seismicity in the Forelands of the Andes

To determine the focal mechanisms and centroid depths of moderate-magnitude earthquakes in the Andean forelands, I used waveform modelling of teleseismic P and SH waves and their depth phases (pP, sP and sS). For earthquakes of $M_w \gtrsim 5.4$, I fit the shape and amplitude of the long-period (15–100 s) teleseismic P and SH waves using the body-waveform inversion algorithm of Zwick et al. [1994]. This method has been used extensively in the region [e.g. Devlin et al., 2012] and yields earthquake centroid depth estimates with uncertainties of ±2–5 km. For earthquakes of $4.8 < M_w < 5.4$ typically only the P waves, and the pP and sP depth phases, are clear on teleseismic seismograms. I calculated the depths of these smaller-magnitude earthquakes by fitting synthetic waveforms to either broadband vertical-component seismograms, or to a stack of short-period vertical-component

seismograms recorded at small-aperture seismic arrays [e.g. Craig et al., 2012]. This method can typically constrain the centroid depth to within ±1–3 km. All of these methods have been described extensively in the literature [e.g. Molnar and Lyon-Caen, 1989; Taymaz et al., 1990; Craig et al., 2011], therefore further details regarding the data processing, inversion strategy, the velocity structure used and the modelling uncertainties are provided in Supplementary Text S1.

In addition to my own modelling of 45 new earthquakes (see Supplementary Table 1 and Supplementary Figures 4–50), I compiled 108 earthquake focal mechanisms and centroid depths derived using similar methods from the literature [Suarez et al., 1983; Chinn and Isacks, 1983; Kadinsky-Cade et al., 1985; Assumpção and Suarez, 1988; Assumpção and Araujo, 1993; Alvarado et al., 2005; Alvarado and Beck, 2006; Meigs and Nabelek, 2010; Devlin et al., 2012; Wimpenny et al., 2018]. Microseismicity located using local seismometer networks provide additional constraints on the depth extent of seismicity within the forelands [Smalley and Isacks, 1990; Cahill et al., 1992; Dorbath et al., 1986; Legrand et al., 2005; Dimate et al., 2003; Vaca et al., 2019]. The resulting compilation of earthquakes is shown in Figure 1 along with the distribution of the Moho depth in the forelands, which varies between 35 km and 48 km [Assumpção et al., 2013; Poveda et al., 2015; Condori et al., 2017]. I describe the along-strike variation in the earthquake focal mechanisms and centroid depths below.

Throughout the northern Andes of Venezuela, Colombia and Ecuador, ∼N-S to ∼NE-SW striking reverse and strike-slip faulting is mostly concentrated along the range front and extends from 5–49 km depth. Aftershocks recorded by temporary seismometer deployments in Colombia [Dimate et al., 2003] and Ecuador [Legrand et al., 2005] following M_w 6 earthquakes located microseismicity down to 30 km. Seismicity deeper than 30 km is only found in a cluster of four earthquakes with centroid depths between 34 km and 49 km depth that ruptured faults within the Garzon Massif of south-central Colombia (Figure 1b,c). These four earthquakes do not appear to be representative of the depth extent of seismicity across the whole northern Andes, as elsewhere both moderate-magnitude earthquakes and microseismicity are consistently confined to depths of less than 30 km.

Earthquakes east of the range front in Colombia have shallow (<20 km) normal-faulting mechanisms, indicating that the top of the foreland crust is in extension. These normal-faulting earthquakes have previously been interpreted to reflect the bending of the foreland lithosphere under the weight of the Andes [Wimpenny et al., 2018]. At a similar distance east of the range front of the Ecuadorian Andes, the shallow crust at 15 km depth is in compression. Therefore the stress state within the top 20 km of the foreland crust varies along strike, as well as perpendicular to strike.

In northern and central Peru, the forelands are characterised by reverse-faulting earthquakes that extend throughout the crust from 5–42 km depth. The same depth distribution of earthquakes has also been observed by a temporary seismometer deployment that recorded microseismicity down to 45 km depth beneath the forelands of central Peru [Dorbath et al., 1986; Suárez et al., 1990]. Although the majority of the earthquakes are concentrated beneath the steep topography along the eastern margin of the Andes, a significant number lie well into the foreland forming a ∼300 km-wide zone of distributed compressional deformation. This zone of distributed deformation coincides with crystalline basement highs that have been uplifted relative to the foreland basin sediments during the Neogene (e.g. the Contoya Arch; see Kley et al. [1999]).

There have been few earthquakes in the sub-Andean fold-thrust belt that wraps around the margins of the central Andean plateau in southern Peru and Bolivia. The largest earthquakes accommodate low-angle thrust faulting at depths ≤20 km, whilst the lower 10–20 km of the foreland crust has experienced only one moderate-magnitude earthquake in the last 50 years — a reverse-faulting earthquake at 31 km depth. A 7 km deep, normal-faulting earthquake east of the range front in southern Peru indicates that the shallow part of the foreland crust is in extension. Geodetic, seismological and structural observations suggest that the foreland crystalline basement is underthrusting the central Andean plateau along a shallowly-dipping décollement in this region [Allmendinger and Gubbels, 1996].

A sharp transition in the foreland seismicity occurs across the Bolivia-Argentina border. At latitude 23°S, the foreland transitions from being predominantly aseismic within the Bolivian sub-Andes to the north, to experiencing frequent ∼N-S striking reverse- and low-angle thrust-faulting earthquakes in the Santa Barbara Ranges to the south. Across the same section of foreland, the trains of closely-spaced anticlines that characterise the surface morphology in the Bolivian sub-Andes abruptly stop, and the foreland structures transition southwards into widely-spaced, east and west-verging reverse faults in the Santa Barbara Ranges [Kley and Monaldi, 2002]. Microseismicity and moderate-magnitude earthquakes beneath Santa Barbara have been recorded down to 35 km depth [Cahill et al., 1992].

South of latitude 26°S, the seismicity becomes more spatially distributed over an area that stretches 300–400 km from the margins of the Andes into the foreland, coincident with the basement uplifts of the Sierra Pampeanas [Jordan et al., 1983]. The focal mechanisms indicate that the earthquakes are predominantly on ∼N-S striking reverse-faults, with a component of strike-slip faulting on ∼N–S or ∼E–W striking planes. Most of the moderate-magnitude seismicity and microseismicity is concentrated between 10 km and 30 km depth, but seismicity does extend to a maximum of 40 km depth beneath the forelands [Smalley and Isacks, 1990].

The along-strike variability in the depth distribution of seismicity within the Andean forelands is consistently mirrored by the microseismicity recorded by local seismometer networks, indicating that the variations are real and are not related to limited sampling of infrequent moderate-magnitude earthquakes (Figure 2). The centroid depth distributions show a single peak within the mid-crust [Chinn and Isacks, 1983], and all of the seismicity is contained within a single layer that is similar in thickness to the crust (Figure 2). These observations are consistent with faults supporting the forces acting through the foreland lithosphere via resistance to slip in a seismogenic layer, which varies from 30 km thick in the northern Andes to 40–45 km thick in the central Peru and the southern Andes. The seismogenic layer is underlain by a mostly aseismic mantle lithosphere [e.g. Maggi et al., 2000b]. In addition to the along-strike variability in the thickness of the seismogenic layer (Figure 1c), there is clear map-view variability in the frequency and spatial distribution of earthquakes that correlates with the deformation style in the foreland. I explore this link further in the next section.

3 Relationship Between Seismicity and Foreland Structure

The influence of pre-Andean deformation structures, particularly those associated with Mesozoic rifting, on the location and style of active shortening is seen throughout the Andean forelands [e.g. Kley et al., 2005; Mora et al., 2006]. These continental rifts were active between the late Permian and the Cretaceous, and developed in response to the break up of Pangea [Spikings et al., 2016]. Figure 3 shows the locations of the major Mesozoic rift-related faults mapped by Ramos [2009] and McGroder et al. [2015] based on seismic reflection data and geological outcrop, and their relationship with the foreland seismicity and the structural style of deformation.

Within northern and central Peru, and in the Sierra Pampeanas of Argentina, the Mesozoic rift systems form ∼300 km wide belts of range-parallel faults that extend from the eastern margin of the high Andes into the foreland. In these regions, the forelands are associated with distributed upper- and lower-crustal compressional earthquakes that closely follows the map-view shape of the rift systems. At the surface the deformation is mostly characterised by 'thick-skinned' structures, with crystalline basement being exhumed towards the surface along steeply-dipping reverse faults [Kley et al., 1999]. In the Marañon Basin of northern Peru and the Argentinian Precordillera, the rift systems trend beneath superficial 'thin-skinned' fold-thrust belts characterised by closely-spaced trains of anticlines formed of sediments, whilst the lower crust beneath these fold-thrust belts remains highly seismogenic.

In the northern Andes of Ecuador, Colombia and Venezuela, the Mesozoic rift systems trend through

the mountain range and parallel to the eastern range front of the Andes, but do not extend more than ∼50 km into the forelands. The distribution of seismicity mirrors this pattern, with reverse and strike-slip faulting earthquakes mostly clustering beneath the range front. In some cases, recent earthquakes beneath the range front can even be directly linked to inverted normal fault structures mapped at the surface or in seismic reflection profiles [e.g. Legrand et al., 2005; Mora et al., 2006].

Beneath the Santa Barbara Ranges of northern Argentina, the western branch of the Salta Rift consists of basins bound by ∼N-S striking normal faults that trend beneath the Andean range front. The same region has experienced a number of moderate-magnitude earthquakes on ∼N-S striking reverse faults and shows evidence for normal-fault reactivation in outcrop [Kley et al., 2005]. However, in the eastern branch of the Salta Rift, where the rift-related faults strike ∼E-W and are almost perpendicular to the range front, there have been no recent moderate-magnitude earthquakes. Therefore, the Mesozoic rifts appear to only be associated with moderate-magnitude earthquakes if the inherited normal faults and rift fabrics strike sub-parallel to the range front.

In contrast to the northern and southern Andes, within southern Peru and Bolivia the Mesozoic rift systems trend through the interior of the central Andean plateau [e.g. Sempere et al., 2002], and rifted basement is mostly absent beneath the range front (Figure 3a). Around the margins of the plateau, the thin-skinned sub-Andean fold-thrust belt has experienced far fewer earthquakes than the northern and southern Andean forelands, and the largest earthquakes are shallow, low-angle thrust faulting events. East of the range front, there have only been two earthquakes; the shallowest being a normal-faulting earthquake with a centroid depth of 7 km, and the deepest being a reverse-faulting earthquake with a centroid depth of 31 km. The same pattern of seismicity has been recognised in the Indian forelands south of Tibet [e.g. Molnar et al., 1977], and is interpreted to reflect bending of the lithosphere in response to the vertical load of the mountain belt.

The remarkable spatial correlation between regions of frequent lower-crustal earthquakes, the Mesozoic rift systems, and the shortening style within the forelands suggests a physical link. The simplest explanation is that, along the margins of the northern and southern Andes, range-parallel normal faults inherited from the Mesozoic rifts are being reactivated throughout the crust as reverse faults, causing the whole seismogenic layer to break up in compression. A summation of the earthquake moment tensors in these regions using the method of Kostrov [1974] suggests that 40–100% of the range-perpendicular shortening rates measured from GPS can be accounted for by seismogenic slip on faults (Table 1). In contrast, around the central Andean plateau the range-perpendicular shortening rates from recent seismicity are 0.5–25% of the rates inferred from GPS (Table 1). Beneath the

sub-Andes, the foreland is presumably too strong to deform significantly in response to the forces associated with mountain building. Therefore, instead of the foreland seismogenic layer breaking up in compression, it is bending and being thrust beneath the central Andean plateau as a relatively rigid plate. Shortening is accommodated by slip on a décollement that separates the rigid foreland from the overlying sub-Andean fold-thrust belt [Allmendinger and Gubbels, 1996].

4 Strength of Inherited Faults in the Forelands

The pattern of seismicity in the forelands of the northern and southern Andes demonstrates that faults inherited from Mesozoic rifts are breaking in reverse-faulting earthquakes, implying that the forces acting on these structures exceeds their frictional resistance to slip. In this section, I estimate the forces acting on these faults and place bounds on their frictional properties.

Gravity acting on differences in the thickness and density of the crust and mantle lithosphere between the Andes and its forelands generates a horizontal buoyancy force F_b that must be balanced by a horizontal force acting through the foreland lithosphere F_f, and resistance to deformation within the mountains [Molnar and Lyon-Caen, 1988]. It is likely that many parts of the Andes are close to the state of $F_b \approx F_f$, as the highest portions of the mountain range have relatively flat, plateau-like topography [Lamb, 2006]. In addition, in the most rapidly-deforming areas of the high Andes, such as the Cordillera Blanca in central Peru and in the Altiplano of southern Peru, seismicity rates and fault slip rates imply that deviations from $F_b = F_f$ are $\lesssim 0.5$–0.7×10^{12} N per metre along-strike, which is $\lesssim$10–25% of F_b [Wimpenny et al., 2020]. Therefore, to place a bound on the forces acting through the forelands F_f, I calculated the buoyancy forces F_b in seven different regions of the Andes using the method described in Copley and Woodcock [2016], with the range of parameters given in Table 2. The seven different regions were selected to encompass sections of the Andes where deformation within the mountains and forelands, and the height of the mountains, are relatively continuous along-strike.

Within Ecuador, Colombia and northern Peru, where the Andes are 2.8–3.5 km high, the calculated buoyancy forces are 3–4$\times10^{12}$ N/m (Figure 4a). In Ecuador there is evidence for shortening within the high Andes [Alvarado et al., 2014], suggesting the buoyancy forces slightly under-estimate the horizontal force acting through the foreland lithosphere in this region. In central Peru, southern Peru, Bolivia, and the Puna plateau of Argentina, where the Andes are 3.8–4.5 km high, the calculated buoyancy forces are 5–6.5$\times10^{12}$ N/m (Figure 4a). In these areas where the buoyancy forces are largest, the high Andes are either undeforming or extending [Mercier et al., 1992; Cladouhos et al.,

1994; Lamb, 2000], implying that the buoyancy forces slightly over-estimate the horizontal force acting through the foreland lithosphere.

Faults in the forelands will only break in earthquakes if their static frictional resistance to slip is overcome. Therefore, a bound on μ' on faults along the margins of the northern and southern Andes can be estimated from the condition that the horizontal force supported by the foreland seismogenic layer F_{sl} must be less than F_f in these regions [e.g. Copley et al., 2011]. The value of μ' represents the effective coefficient of friction averaged over the fault plane and will be an upper bound, as shear zones beneath the brittle faults will also support some of the force acting through the lithosphere.

The horizontal force that can be transmitted through the seismogenic layer of thickness T_s that contains faults that dip at an angle θ relative to the vertical is given by [Turcotte and Schubert, 2002]:

$$F_{sl} = \frac{\mu' \rho g T_s^2}{\sin 2\theta - \mu'(1 + \cos 2\theta)}, \tag{1}$$

where g is the acceleration due to gravity and ρ is the average density of the layer. Figure 4b shows the predictions of Equation 1 plotted against estimates of F_f and T_s for the seven different regions of the Andes. In the regions where the foreland seismogenic layer is breaking up in compressional earthquakes on inherited normal faults (Colombia, Ecuador, northern Peru, central Peru and the Puna/Sierra Pampeanas of Argentina), Figure 4b demonstrates that the effective coefficient of friction on these inherited faults is consistently $\mu' < 0.2$, and may well be $\lesssim 0.1$. This is equivalent to the faults supporting average shear stresses $\bar{\tau} < 150$ MPa in regions with a 45 km thick seismogenic layer and < 100 MPa in regions with a 30 km thick seismogenic layer. If the faults were any stronger, the forces acting through the foreland would not be large enough to overcome the frictional resistance to slip and break the seismogenic layer in compressional earthquakes. Notably, areas with the thicker foreland seismogenic layer support the higher mountain ranges, as predicted by Maggi et al. [2000a].

Around the margins of central Andean plateau in south Peru and Bolivia, where there are no pre-existing normal faults and the foreland is being thrust beneath the mountain range, the relationship between F_f and T_s is less clear (Figure 4b). It is possible that in these regions either: (1) the seismogenic layer is thicker than estimated by the deepest earthquakes, (2) that μ' on any faults is larger than $\sim$0.1–0.2, or (3) that any faults present may be severely mis-oriented relative to the range front strike for re-activation (Figure 4b) [e.g. Sibson, 1995]. All of these mechanisms would lead to a seismogenic layer that is stronger than the forces acting through the foreland, meaning that the layer is thrust coherently beneath the plateau, as opposed to breaking up through slip on faults. With this

configuration of deformation the force transmitted into the mountain range is no longer limited by faults within the foreland lithosphere, but by the strength of faults along the top of the underthrusting foreland and the viscosity of the plateau interior [Ainscoe et al., 2017; McKenzie et al., 2019].

Many of the earthquakes in the forelands of the northern and southern Andes are M_w 5–6 and do not necessarily break the full seismogenic layer at any one time. In the locations of these smaller-magnitude earthquakes, the forces acting through the lithosphere may get focused onto strong asperities, whilst the remainder of the fault zone supports shear stresses well below the frictional resistance to slip. The force required to break an asperity with down-dip width W and centroid depth z_c can be calculated from Equation 1 by replacing the T_s^2 term with $2z_cW\cos\theta$. Even in the extreme case where all of the force acting through the foreland F_f is focused onto the rupture area of a foreland earthquake, the constraints on the size of this force require that $\mu' \lesssim 0.3$–0.4 in order to generate the $M_w \sim 6$ earthquakes near the base of the 30–45 km thick seismogenic layer (Figure 4c). However, the extreme differences in the stress state in the seismogenic layer assumed by this model are unlikely given that strain must accumulate relatively evenly throughout the layer to load and break the faults, and to account for the frequent earthquakes over the seismogenic layer's entire thickness (Figure 4d).

5 A Dry, Metastable Lower Crust Beneath the Andean Forelands

The frictionally-weak faults within the forelands of the northern and southern Andes remain seismogenic throughout the crust. In this section, I discuss how the depth extent of the seismicity, and the geological history of the inverted rift basins in the forelands, can be used to place constraints on the properties of the lower crust through which these weak faults cut.

A recent re-assessment of the depth distribution of earthquakes within the continents revealed a bimodal pattern that depends on the geological history of the region. Within the Phanerozoic mobile belts (e.g. Tibet, the Aegean, the Basin and Range) faults only remain seismogenic to depths of 10–20 km [Maggi et al., 2000b]. The depth extent of seismicity in these settings is thought to be limited by the onset of thermally-activated creep in hydrated, quartz-dominated rocks at temperatures of 300–400 $^{\circ}C$ [Sibson, 1982]. However, within and along the margins of the Precambrian shields that have resisted significant deformation throughout the Phanerozoic (e.g. India, Africa, Eurasia), seismicity occurs to depths of 40–60 km, extending through the lower crust and, occasionally, into the upper mantle [Maggi et al., 2000b; Jackson et al., 2008]. Temperatures within the seismogenic lower crust of the Precambrian shields are 400–600 $^{\circ}C$ [McKenzie et al., 2005]. Therefore, rocks in the lower

crust beneath the Precambrian shields remain seismogenic and mechanically strong to far higher temperatures than beneath the Phanerozoic mobile belts, indicating that there is some compositional difference between these regions that accounts for their contrasting mechanical properties.

Jackson et al. [2004] argued that the lower crust beneath the Precambrian shields can remain seismogenic and mechanically strong at such high temperature because of its anhydrous ('dry') mineralogy. Where sections of the Precambrian lower crust outcrop at the surface, they are typically formed of dry, granulite-facies rocks [Fountain and Salisbury, 1981]. These ancient granulites formed as a result of high-temperature (>800–900 $°C$) metamorphism, possibly during mountain building [McKenzie and Priestley, 2016], that stripped the rocks of hydrous minerals through melting [Burton and O'Nions, 1990], leaving behind vast areas with an anhydrous, load-bearing mineral assemblage of mainly feldspars and pyroxenes. Psuedotachylytes provide evidence that dry granulite can be seismogenic at lower-crustal conditions [Lund et al., 2004; Hawemann et al., 2018], but even trace amounts of water ingress into these rocks leads to viscous creep and mylonite formation that overprints the ancient granulitic fabrics [Austrheim and Boundy, 1994; Menegon et al., 2017]. These field observations are consistent with laboratory experiments that show the creep strength of feldspars and pyroxenes is drastically reduced by a few hundredths of a weight percent of structurally-bound water at lower-crustal temperatures [Mackwell et al., 1998; Rybacki and Dresen, 2004]. Therefore, a seismogenic and mechanically strong lower crust, like that beneath the Andean forelands, is often considered to be a proxy for a dry, granulitic lower crust [Sloan et al., 2011; Craig and Jackson, 2021].

Direct evidence of the composition of the seismogenic lower crust beneath the Andean forelands comes from xenoliths contained within late Cretaceous basalts that are inter-bedded with the syn-rift sediments of the Metán-Alemania Basin — a sub-basin of the western branch of the Salta Rift [Lucassen et al., 1999] (see Figure 3a for location of the Salta Rift). The xenolith suite consists of pristine felsic and mafic granulites that equilibrated at temperatures of 800–900 $°C$ and pressures of 0.95–1.05 GPa (∼34–38 km). Peridotite xenoliths in the same suite also record temperatures of 1000–1200 $°C$ at pressures of 1.2–1.6 GPa in the shallow lithospheric mantle [Lucassen et al., 2005]. Whole-rock Sm-Nd ages of the crustal xenoliths are 80–90 Ma, which are thought to date the timing of their exhumation during syn-rift volcanism [Lucassen et al., 1999]. These observations suggest that, in the same depth range there is present-day seismicity beneath the Salta Rift, the lower crust was at granulite-facies conditions in the late Cretaceous (see Figure 2 for depth-range comparison).

Present-day conditions within the lower crust beneath the Salta Rift will be lower in pressure and temperature than those during rifting, as a result of the thinning of the radiogenic crust and conductive

cooling of the lithosphere [Sandiford and Powell, 1986]. To estimate the evolution of the P–T conditions beneath the Salta Rift, I ran a series of numerical calculations that simulate the late Cretaceous rifting and subsequent post-rift cooling based on the 1-D thermo-kinematic numerical model of Bown and White [1995] (see Supplementary Text S2 for details of the model set-up). I used a grid-search approach to find models that matched the P–T–t constraints from xenolith thermobarometry, the history of syn- and post-rift sedimentation within the Metán-Alemania basin [Salfity and Marquillas, 1994; Starck, 2010], and the present-day crust and lithospheric mantle thickness. I then used the models that fit these varied data to explore the possible P–T–t evolution of the seismogenic lower crust (Figure 5).

During rifting, the geotherm was perturbed away from a steady state and rocks were advected towards the surface causing a pressure decrease (ΔP). The amplitude of ΔP is controlled primarily by the amount of crustal stretching. At this time the lower crust was hot enough to undergo the dehydration-melting reactions necessary to form granulite-facies rocks at depths of ∼35 km (Figure 5a). The high lower-crustal temperatures could be achieved in the modelling by significant syn-rift thinning of the lithospheric mantle [e.g. Hopper et al., 2020], or an initially hot geotherm due to a thick radiogenic crust or thin lithospheric mantle. However, the limited amount of felsic magmatism recorded within the syn-rift sediments [Salfity and Marquillas, 1994] implies that the lower crust was already mostly dry by the Cretaceous in order to avoid widespread melting. Subsequent post-rift cooling over ∼80–90 Myrs led to a decrease in temperature (ΔT) throughout the lower crust. For rocks exhumed to a depth of 35 km, the models estimate that ΔT = 75–250 $^{\circ}C$ and ΔP = 0.15–0.25 GPa (Figure 5b,c). Estimates of the present-day temperatures at 35 km depth beneath the Salta Rift are 600–700 $^{\circ}C$ (Figure 5a), with the lower crust still cooling towards steady state.

The xenolith data and rift models suggest that, if the lower crust beneath the western branch of the Salta Rift was not already formed of dry granulite, then the P-T conditions in the late Cretaceous will have led to widespread granulite-facies metamorphism. A modern analogue of the Cretaceous Salta Rift may be the Rio Grande Rift [Cipar et al., 2020]. The lower crust has subsequently cooled to amphibolite-facies conditions. Despite the significant changes in P and T, the dry granulites within the lower crust are likely to have remained metastable, as the possible retrograde reactions have sluggish kinetics in the absence of the volatiles that were driven off by melting and melt segregation along their prograde path [Brown, 2002]. The geological evolution of the Salta Rift is therefore consistent with the view that, where the lower crust is seismogenic along the margins of the Andes, it is formed of dry, granulitic rocks that preserve a metastable mineral assemblage [Jackson et al., 2021].

6 Discussion

6.1 Structural Inheritance and Mountain Building in the Andes

Along-strike differences in the mechanical properties of the foreland lithosphere inherited from past deformation episodes have been suggested to influence the first-order structure of the Andes [e.g. Watts et al., 1995; Kley et al., 1999]. I have shown that, where Mesozoic rifts lie along the range front, the foreland crust is highly seismogenic and is deforming entirely in compressional earthquakes (Figure 6, top). Frictionally-weak reverse faults are accommodating the majority of the shortening within the foreland crust, though these faults are occasionally obscured at the surface by aseismic fold-thrust belts formed in the sedimentary cover. Where shortening is taking place on inherited faults that cut through the whole crust, the Andes form a narrow, linear mountain belt, and the strength of seismogenic layer is controlling the height of the mountains (Section 4).

Where the Mesozoic rifts are internal to the mountain range, the foreland crust is relatively aseismic. I have demonstrated that the pattern of earthquakes implies the seismogenic layer is too strong to break up in compression, so is bending and underthrusting the mountain range coherently beneath a low-angle décollement (Figure 6, bottom). Where the foreland is underthrusting the mountain range, the Andes form a high elevation, low-relief plateau that is gently curved in plan view. In this setting, the force balance is no longer limited by the strength of the foreland seismogenic layer, but by the strength of faults along the top of the underthrusting lithosphere and the viscous resistance to underthrusting beneath the plateau [e.g. Ainscoe et al., 2017; McKenzie et al., 2019].

The interpretation described above implies that the mechanical properties of the rifted lithosphere have not only affected the style of active deformation in the forelands, but also the structure and shape of the mountain belt. Therefore, determining why the seismogenic layer in the rifted lithosphere can break up, whilst in un-rifted lithosphere it cannot, is key to understanding the controls on the growth and evolution of the Andes.

One possibility is that the seismogenic layer is thicker around the margins of the central Andean plateau than in the northern and southern Andes, meaning it is too strong to break. This hypothesis can be tested using the depth distribution of earthquakes. Seismicity within the forelands of the northern and southern Andes extends down to 30–45 km, whilst around the margins of the central Andean plateau seismicity has only been recorded to 31 km depth. The sparse seismicity in the forelands of the plateau, however, precludes a robust estimate on the seismogenic thickness, and 31

km is a lower bound. Local seismicity studies [e.g. Smalley and Isacks, 1990; Suárez et al., 1990] are needed to provide a more robust estimate of the seismogenic thickness in this area. Nonetheless, on the basis of the available observations, although along-strike variability in the thickness of the seismogenic layer is controlling the height of the Andes mountains in some areas, it does not appear to control the shortening style in the Andean forelands.

Along-strike changes in the thickness of the foreland lithosphere determined from surface-wave tomography [e.g. Priestley and McKenzie, 2013] also do not appear to correlate with the shape of the Andes, or the style of shortening in the forelands (Supplementary Figure 3). However, the horizontal resolution of the tomography (∼300 km), and the possibility of horizontal smearing of velocity anomalies associated with the subducting Nazca Plate, precludes any confident comparison of lithospheric thickness and shortening style in the Andean forelands.

The explanation that is most consistent with the observations available is that the small amount of extension during Mesozoic rifting (β-factor $<$ 1.2–1.3) formed or reactivated weak, ∼N–S striking faults in the otherwise strong, dry crust along the western margin of the Precambrian shields in South America. The thermal effects from rifting in all but the youngest of the rift systems will have dissipated through conductive cooling over the last ∼100–300 Myrs. As a result, the presence or absence of weak faults that are well-oriented relative to the range front for failure is likely the primary control on the along-strike variability in the style of shortening along the margins of the Andes.

The locus of shortening in the Andes is stepping eastwards through time [McQuarrie, 2002; Barke and Lamb, 2006; Oncken et al., 2006]. Therefore, the difference between the linear, narrow mountain ranges of the northern and southern Andes, and the wide, curved central Andean plateau, may simply reflect mountain ranges in different stages of their evolution [Wimpenny et al., 2018]. Once shortening within the forelands of the northern and southern Andes advances eastwards out of the Mesozoic rift systems and onto un-rifted foreland lithosphere, then the deformation style may switch from crustal shortening along inherited faults to continental underthrusting [Kley et al., 1999]. The onset of underthrusting in Bolivia is believed to have led to rapid crustal thickening along the margin of the Andes and the formation of the central Andean plateau in the late Miocene [Barke and Lamb, 2006]. In this sense, the mechanical properties of the foreland lithosphere inherited from Mesozoic rifting have imparted a strong influence on the growth and evolution of the Andes by controlling the style of shortening along the margins of the mountain range [Allmendinger et al., 1983; Watts et al., 1995; Kley et al., 1999]. This study advances our understanding of this process by demonstrating that the frictional properties of faults, and the strength of the seismogenic layer in the foreland lithosphere, are the key mechanical

properties in controlling these various styles of mountain building in the Andes.

6.2 Weak, Seismogenic Faults in a Strong, Dry Lower Crust

Two mechanisms have been invoked to account for weak faults in the upper crust: (1) highly-pressurised water within the fault core, and (2) intrinsically-weak phyllosilicate minerals within faults that are produced through water-mediated alteration of the fault rock. However, the lower crust is thought to be extremely dry in order to remain mechanically strong and seismogenic [Jackson et al., 2004]. In this section, I critically assess whether the same, water-mediated mechanisms weakening faults in the upper crust could control the frictional properties of seismogenic faults in the lower crust.

The dry, granulitic wall rocks inferred to surround faults in the forelands of the Andes will be metastable at lower-crustal conditions, and will readily react with free water to form new, stable mineral assemblages. The composition of the lower crust should therefore act as a sink of water and buffer the water pressure to far below lithostatic over time, except in regions of pervasive water influx and retrogression [Yardley and Valley, 1997]. The rates of hydration reactions from natural analogues suggest water can be consumed by dry granulitic rocks at mid-crustal temperature conditions at $\sim 10^{-8}$ g/cm^2/s [Whyte et al., 2021]. Without some mechanism that can isolate free water within the fault core from the reactive wall rocks, it is therefore unlikely that a pervasive water phase at 60–80% of lithostatic pressure is the cause of the frictionally-weak faults in the lower crust.

If pervasive water influx does occur into a fault zone formed of dry granulite at amphibolite-facies conditions, it will lead to water-consuming reactions that form hydrous minerals, particularly amphiboles and phyllosilicates [e.g. Beach, 1976; Andersen et al., 1991]. A common feature of exhumed granulite terrains are shear zones that contain aligned hydrous minerals surrounded by anhydrous wall rocks that preserve ancient fabrics [e.g. Sørensen, 1983; Newton, 1990; Austrheim and Boundy, 1994; Getsinger et al., 2013; Menegon et al., 2017]. This widespread observation implies that water ingress into fault zones during deformation leads to reaction softening and the onset of viscous creep at lower-crustal conditions, precluding the accumulation of elastic strain and frictional slip. The seismogenic fault zones in the Andean forelands are interpreted to have been re-activated following Mesozoic rifting, and presumably have a protracted history of deformation over millions of years that would have caused water ingress and reaction softening if there was water available in the lower crust. Therefore an alternative, water-absent mechanism may be necessary to account for the frictional properties of faults within the lower crust of the Andean forelands. Below I discuss some possible alternatives.

Shear zones within lower-crustal terrains often form networks of fine-grained or hydrated rocks in outcrop that wrap around rigid, undeformed blocks [e.g. Sørensen, 1983]. It is possible that earthquakes nucleate at stress concentrations in these mechanically heterogeneous fault zones by rupturing the rigid blocks (Figure 6, box 1). Although this mechanism can certainly account for small earthquakes [Campbell et al., 2020], for moderate-magnitude earthquakes with kilometre-sized rupture areas like those in the Andean forelands, even if all of the force acting through the lithosphere were focused onto the rupture area, the faults must still have an effective coefficient of friction less than half that predicted by Byerlee's Law (see the calculations presented in Section 4). Otherwise, the faults within the rigid blocks would be too strong to break, given the constraints on the size of the force acting through the foreland lithosphere.

Alternatively, fluids rich in non-hydrous volatile phases (e.g. N_2, CO_2) may be present as intergranular films and in pores in lower-crustal fault zones [Andersen et al., 1990]. Non-hydrous volatiles can reduce the activity of water in any fluid that may exist, which helps stabilise the anhydrous mineral assemblage of granulites that is needed for elastic strain to accumulate at high temperatures. The volatiles may also become highly-pressurised through deformation compaction and reduce the effective stresses within the fault zone without lowering the creep strength of the rock (Figure 6, box 2). Few experimental constraints exist on the influence of non-hydrous volatiles on creep in silicate minerals, which limits any quantitative test of this mechanism. Nonetheless, evidence from exhumed psuedotachylytes suggest that CO_2-rich fluids are associated with frictional slip in mafic granulites at lower-crustal conditions [Sørensen et al., 2019].

It is also possible that the conditions under which friction is measured in the laboratory are just too far removed from those experienced by lower-crustal fault zones, and that dry fault rocks are intrinsically frictionally-weak at high confining pressures and temperatures (Figure 6, box 3). For example, if frictional resistance is governed by microscopic surface roughness, then the high temperatures and long inter-event times in the lower crust may allow asperities on fault surfaces to relax through localised creep, producing smooth and frictionally-weak faults. This explanation circumvents the need for a free fluid phase all together, and would account for the observation that psuedotachylytes can occur in completely dry lower-crustal rocks [Hawemann et al., 2019; Dunkel et al., 2021]. However, the same asperity relaxation effects have been shown to cause a transition from velocity-weakening (i.e. seismogenic) to velocity-strengthening (i.e. aseismic) slip behaviour in olivine aggregates deformed at high temperatures [Boettcher et al., 2007], which may in fact preclude lower-crustal seismicity.

It therefore remains unclear which, if any, of these mechanisms may account for the mechanical prop-

erties of faults in the Andean forelands. Testing the different hypotheses shown in Figure 6 using geological observations is difficult, as the various mechanisms are highly dependent on the mineralogy, fluid availability and fluid composition, which will all vary along the fault. In contrast, the geophysical constraints developed in this study reflect fault-averaged mechanical properties over length-scales of kilometres, which undoubtedly smooth out complex, outcrop-scale structure and processes. Nonetheless, a few simple conclusions regarding the mechanics of lower-crustal fault zones can be drawn from this discussion: (1) frictionally-weak faults may remain seismogenic in the continental lower crust after multiple episodes of reactivation separated by millions of years, and (2) water-assisted weakening mechanisms like those inferred to be active in the upper crust are unlikely to operate on seismogenic faults within a dry lower crust.

7 Conclusions

I have shown that the distribution of seismicity along the margin of the Andes is correlated with the locus of Mesozoic rift systems that stretched the foreland lithosphere prior to the Andean orogeny. Where the rift systems lie along the margins of the mountain belt, the whole 30–45 km-thick seismogenic layer is shortening by slip on inherited normal faults. Where these inherited faults are absent, or mis-oriented relative to the shortening direction, the foreland is bending and being underthrust beneath the Andes. I have estimated the forces acting on the inherited faults, and demonstrated that they have an effective coefficient of static friction $\mu' < 0.2$, which is significantly lower than predicted by laboratory experiments. The mechanisms that have been proposed to generate weak, seismogenic faults in the upper crust are typically related to a free water-phase. I argue that these water-assisted mechanisms alone are unlikely to weaken faults in the seismogenic lower crust due to its dry, granulitic composition. Therefore, although the frictional properties of faults within the Andean forelands appear to be important in controlling the style of mountain building, the geological controls on their mechanical properties remain enigmatic.

Acknowledgements

SW was supported by the Denman Baynes Senior Studentship at Clare College, Cambridge. SW thanks Alex Copley, Carlos Benavente, David Wallis, Aisling O'Kane and Camilla Penney for discussions and comments on the manuscript.

Data Availability

Waveform data used in this study was is freely available from the Incorporated Research Institute for Seismology (IRIS) data management centre. The computer codes used to perform the force-balance calculations and the 1-D thermo-kinematic modelling are available from: `https://github.com/samwimpenny/forelands_2021`. All earthquake focal mechanism data will be uploaded to the gWFM catalogue available at: `https://comet.nerc.ac.uk/gwfm_catalogue/gWFM_catalogue.html`

References

Ainscoe, E. A., Elliott, J. R., Copley, A., Craig, T. J., Li, T., Parsons, B. E., and Walker, R. T. (2017). Blind Thrusting, Surface Folding, and the Development of Geological Structure in the Mw6.3 2015 Pishan (China) Earthquake. *Journal of Geophysical Research: Solid Earth*, 122(11):9359–9382.

Allmendinger, R. and Gubbels, T. (1996). Pure and simple shear plateau uplift, Altiplano-Puna, Argentina and Bolivia. *Tectonophysics*, 259(1-3):1–13.

Allmendinger, R. W., Ramos, V. A., Jordan, T. E., Palma, M., and Isacks, B. L. (1983). Paleogeography and Andean structural geometry, northwest Argentina. *Tectonics*, 2(1):1–16.

Alvarado, A., Audin, L., Nocquet, J. M., Lagreulet, S., Segovia, M., Font, Y., Lamarque, G., Yepes, H., Mothes, P., Rolandone, F., Jarrín, P., and Quidelleur, X. (2014). Active tectonics in Quito, Ecuador, assessed by geomorphological studies, GPS data, and crustal seismicity. *Tectonics*, 33(2):67–83.

Alvarado, P. and Beck, S. (2006). Source characterization of the San Juan (Argentina) crustal earthquakes of 15 January 1944 (Mw 7.0) and 11 June 1952 (Mw 6.8). *Earth and Planetary Science Letters*, 243(3-4):615–632.

Alvarado, P., Beck, S., Zandt, G., Araujo, M., Triep, E., Isacks, B. L., Araujo, M., Puebla, N. P., and Sistena, J. A. (2005). Crustal deformation in the south-central Andes backarc terranes as viewed from regional broad-band seismic waveform modelling. *Geophysical Journal International*, 163(2):580–598.

Andersen, T., Austrheim, H., and Burke, E. A. (1991). Fluid-induced retrogression of granulites in the Bergen Arcs, Caledonides of W. Norway: Fluid inclusion evidence from amphibolite-facies shear zones. *LITHOS*, 27(1):29–42.

Andersen, T., Austrheim, H., and Burke, E. A. J. (1990). Fluid inclusions in granulites and eclogites from the Bergen Arcs, Caledonides of W. Norway. *Mineralogical Magazine*, 54(375):145–158.

Assumpção, M. and Araujo, M. (1993). Effect of the Altiplano-Puna plateau, South America, on the regional intraplate stresses. *Tectonophysics*, 221(3-4):475–496.

Assumpção, M., Feng, M., Tassara, A., and Julià, J. (2013). Models of crustal thickness for South America from seismic refraction, receiver functions and surface wave tomography. *Tectonophysics*, 609:82–96.

Assumpção, M. and Suarez, G. (1988). Source mechanisms of moderate-size earthquakes and stress orientation in mid-plate South America. *Geophysical Journal International*, 92(2):253–267.

Austrheim, H. and Boundy, T. M. (1994). Pseudotachylytes generated during seismic faulting and eclogitization of the deep crust. *Science*, 265(5168):82–83.

Barke, R. and Lamb, S. (2006). Late Cenozoic uplift of the Eastern Cordillera, Bolivian Andes. *Earth and Planetary Science Letters*, 249(3-4):350–367.

Beach, A. (1976). The Interrelations of Fluid Transport , Deformation , Geochemistry and Heat Flow in Early Proterozoic Shear Zones in the Lewisian Complex Author (s): A . Beach Source : Philosophical Transactions of the Royal Society of London . Series A , Mathematical. *Philosophical Transactions of the Royal Society A*, 280(1298):569–604.

Boettcher, M. S., Hirth, G., and Evans, B. (2007). Olivine friction at the base of oceanic seismogenic zones. *Journal of Geophysical Research: Solid Earth*, 112(1):1–13.

Bown, J. W. and White, R. S. (1995). Effect of finite extension rate on melt generation at rifted continental margins. *Journal of Geophysical Research*, 100(B9):18011–18029.

Brown, M. (2002). Retrograde processes in migmatites and granulites revisited. *Journal of Metamorphic Geology*, 20(1):25–40.

Bürgmann, R. and Dresen, G. (2008). Rheology of the Lower Crust and Upper Mantle: Evidence from Rock Mechanics, Geodesy, and Field Observations. *Annual Review of Earth and Planetary Sciences*, 36:531–567.

Burton, K. W. and O'Nions, R. K. (1990). The timescale and mechanism of granulite formation at Kurunegala, Sri Lanka. *Contributions to Mineralogy and Petrology*, 106(1):66–89.

Butler, R. W., Tavarnelli, E., and Grasso, M. (2006). Structural inheritance in mountain belts: An Alpine-Apennine perspective. *Journal of Structural Geology*, 28(11):1893–1908.

Byerlee, J. (1978). Friction of rocks. *Pure and Applied Geophysics*, 116(4-5):615–626.

Cahill, T., Isacks, B. L., Whitman, D., Chatelain, J. ., Perez, A., and Chiu, J. M. (1992). Seismicity and tectonics in Jujuy Province, northwestern Argentina. *Tectonics*, 11(5):944–959.

Campbell, L. R., Menegon, L., Fagereng, and Pennacchioni, G. (2020). Earthquake nucleation in the lower crust by local stress amplification. *Nature Communications*, 11(1):1–9.

Chinn, D. S. and Isacks, B. L. (1983). Accurate source depths and focal mechanisms of shallow earthquakes in western South America and in the New Hebrides Island Arc. *Tectonics*, 2(6):529–563.

Cipar, J. H., Garber, J. M., Kylander-Clark, A. R., and Smye, A. J. (2020). Active crustal differentiation beneath the Rio Grande Rift. *Nature Geoscience*, 13(11):758–763.

Cladouhos, T. T., Allmendinger, R. W., Coira, B., and Farrar, E. (1994). Late cenozoic deformation in the Central Andes: fault kinematics from the northern Puna, northwestern Argentina and southwestern Bolivia. *Journal of South American Earth Sciences*, 7(2):209–228.

Collettini, C., Tesei, T., Scuderi, M. M., Carpenter, B. M., and Viti, C. (2019). Beyond Byerlee friction, weak faults and implications for slip behavior. *Earth and Planetary Science Letters*, 519:245–263.

Condori, C., França, G. S., Tavera, H. J., Albuquerque, D. F., Bishop, B. T., and Beck, S. L. (2017). Crustal structure of north Peru from analysis of teleseismic receiver functions. *Journal of South American Earth Sciences*, 76:11–24.

Copley, A. (2018). The strength of earthquake-generating faults. *Journal of the Geological Society*, 174(1).

Copley, A., Avouac, J.-P., Hollingsworth, J., and Leprince, S. (2011). The 2001 Mw 7.6 Bhuj earthquake, low fault friction, and the crustal support of plate driving forces in India. *Journal of Geophysical Research: Solid Earth*, 116(B8):B08405.

Copley, A. and Woodcock, N. (2016). Estimates of fault strength from the Variscan foreland of the northern UK. *Earth and Planetary Science Letters*, 451:108–113.

Craig, T. J., Copley, A., and Jackson, J. A. (2012). Thermal and tectonic consequences of India underthrusting Tibet. *Earth and Planetary Science Letters*, 353-354:231–239.

Craig, T. J. and Jackson, J. A. (2021). Variations in the Seismogenic Thickness of East Africa. *Journal of Geophysical Research: Solid Earth*, 126(3):e2020JB020754.

Craig, T. J., Jackson, J. A., Priestley, K., and McKenzie, D. (2011). Earthquake distribution patterns in Africa: their relationship to variations in lithospheric and geological structure, and their rheological implications. *Geophysical Journal International*, 185(1):403–434.

Devlin, S., Isacks, B. L., Pritchard, M. E., Barnhart, W. D., and Lohman, R. B. (2012). Depths and focal mechanisms of crustal earthquakes in the central Andes determined from teleseismic waveform analysis and InSAR. *Tectonics*, 31(2):1–33.

Dimate, C., Rivera, L., Taboada, A., Delouis, B., Osorio, A., Jimenez, E., Fuenzalida, A., Cisternas, A., and Gomez, I. (2003). The 19 January 1995 Tauramena (Colombia) earthquake: Geometry and stress regime. *Tectonophysics*, 363(3-4):159–180.

Dorbath, C., Dorbath, L., Cisternas, A., Deverchere, J., Diament, M., Ocola, L., and Morales, M. (1986). On crustal seismicity of the Amazonian foothill of the central Peruvian Andes. *Geophysical Research Letters*, 13(10):1023–1026.

Dunkel, K. G., Zhong, X., Arnestad, P. F., Valen, L. V., and Jamtveit, B. (2021). High Transient Stress in The Lower Crust: Evidence from Dry Pseudotachylytes in Granulites, Lofoten Archipelago, Northern Norway. *Geology*, 49(2):135–139.

Fountain, D. M. and Salisbury, M. H. (1981). Exposed cross-sections through the continental crust: implications for crustal structure, petrology, and evolution. *Earth and Planetary Science Letters*, 56(C):263–277.

Getsinger, A. J., Hirth, G., Stünitz, H., and Goergen, E. T. (2013). Influence of water on rheology and strain localization in the lower continental crust. *Geochemistry, Geophysics, Geosystems*, 14(7):2247–2264.

Golonka, J., Lawver, L., Coffin, M., Dalziel, I. D., and Gahagan, L. (1995). Paleogeographic Reconstructions with Sediment Isopachs, PLATES progress report No. 104-0695. Technical report, University of Texas Institute for Geophysics.

Hawemann, F., Mancktelow, N. S., Pennacchioni, G., Wex, S., and Camacho, A. (2019). Weak and Slow, Strong and Fast: How Shear Zones Evolve in a Dry Continental Crust (Musgrave Ranges, Central Australia). *Journal of Geophysical Research: Solid Earth*, 124(1):219–240.

Hawemann, F., Mancktelow, N. S., Wex, S., Camacho, A., and Pennacchioni, G. (2018). Pseudotachylyte as field evidence for lower-crustal earthquakes during the intracontinental Petermann Orogeny (Musgrave Block, Central Australia). *Solid Earth*, 9(3):629–648.

Hopper, E., Gaherty, J. B., Shillington, D. J., Accardo, N. J., Nyblade, A. A., Holtzman, B. K., Havlin, C., Scholz, C. A., Chindandali, P. R., Ferdinand, R. W., Mulibo, G. D., and Mbogoni, G. (2020). Preferential localized thinning of lithospheric mantle in the melt-poor Malawi Rift. *Nature Geoscience*, 13(8):584–589.

Hubbert, M. K. and Rubey, W. W. (1959). Mechanics of fluid-filled porous solids and its application to overthrust faulting. *Bulletin of the Geological Society of America*, 70(2):115–166.

Imber, J., Holdsworth, R. E., Butler, C. A., and Lloyd, G. E. (1997). Fault-zone weakening processes along the reactivated Outer Hebrides Fault Zone, Scotland. *Journal of the Geological Society*, 154(1):105–109.

Jackson, J. (2002). Faulting, flow, and the strength of the continental lithosphere. *International Geology Review*, 44(1):39–61.

Jackson, J., McKenzie, D., and Priestley, K. (2021). Relations between earthquake distributions, geological history, tectonics and rheology on the continents. *Philosophical Transactions of the Royal Society A: Mathematical, Physical and Engineering Sciences*, 379(2193).

Jackson, J. A., Austrheim, H., McKenzie, D., and Priestley, K. (2004). Metastability, mechanical strength, and the support of mountain belts. *Geology*, 32(7):625.

Jackson, J. A., McKenzie, D., Priestley, K., and Emmerson, B. (2008). New views on the structure and rheology of the lithosphere. *Journal of the Geological Society*, 165(2):453–465.

Jordan, T. E., Isacks, B. l., Allmendinger, R. E., Brewer, J. A., Ramos, V. A., and Ando, C. J. (1983). Andean tectonics related to geometry of subducted Nazca plate. *Geological Society of America Bulletin*, 94(3):341.

Kadinsky-Cade, K., Reilinger, R., and Isacks, B. (1985). Surface deformation associated with the November 23, 1977, Caucete, Argentina, earthquake sequence. *Journal of Geophysical Research: Solid Earth*, 90(14):12691–12700.

Kendrick, E., Bevis, M., Smalley, R., and Brooks, B. (2001). An integrated crustal velocity field for the central Andes. *Geochemistry, Geophysics, Geosystems*, 2.

Kendrick, E., Brooks, B. A., Bevis, M., Jr., R. S., Lauria, E., Araujo, M., and Parra, H. (2006). Orogenia activa de los Andes centro-australes estudiada mediante geodesia de GPS. *Revista de la Asociación Geológica Argentina*, 61(4):555–566.

Kley, J. and Monaldi, C. R. (2002). Tectonic inversion in the Santa Barbara System of the central Andean foreland thrust belt, northwestern Argentina. *Tectonics*, 21(6):11–1–11–18.

Kley, J., Monaldi, C. R., and Salfity, J. A. (1999). Along-strike segmentation of the Andean foreland: Causes and consequences. *Tectonophysics*, 301(1-2):75–94.

Kley, J., Rossello, E. A., Monaldi, C. R., and Habighorst, B. (2005). Seismic and field evidence for selective inversion of Cretaceous normal faults, Salta rift, northwest Argentina. *Tectonophysics*, 399(1-4 SPEC. ISS.):155–172.

Kostrov, B. V. (1974). Seismic moment and energy of earthquakes, and seismic flow of rock. *Physics of the Solid Earth*, 1:13–21.

Lamb, S. (2006). Shear stresses on megathrusts: Implications for mountain building behind subduction zones. *Journal of Geophysical Research: Solid Earth*, 111(B7):B07401.

Lamb, S. H. (2000). Active deformation in the Bolivian Andes, South America. *Journal of Geophysical Research: Solid Earth*, 105(B11):25627–25653.

Legrand, D., Baby, P., Bondoux, F., Dorbath, C., Bès de Berc, S., and Rivadeneira, M. (2005). The 1999-2000 seismic experiment of Macas swarm (Ecuador) in relation with rift inversion in Subandean foothills. *Tectonophysics*, 395(1-2):67–80.

Lucassen, F., Franz, G., Viramonte, J., Romer, R. L., Dulski, P., and Lang, A. (2005). The late Cretaceous lithospheric mantle beneath the Central Andes: Evidence from phase equilibria and composition of mantle xenoliths. *Lithos*, 82(3-4):379–406.

Lucassen, F., Lewerenz, S., Franz, G., Viramonte, J., and Mezger, K. (1999). Metamorphism, isotopic ages and composition of lower crustal granulite xenoliths from the Cretaceous Salta Rift, Argentina. *Contributions to Mineralogy and Petrology*, 134(4):325–341.

Lund, M. G., Austrheim, H., and Erambert, M. (2004). Earthquakes in the deep continental crust-insights from studies on exhumed high-pressure rocks. *Geophysical Journal International*, 158(2):569–576.

Mackwell, S. J., Zimmerman, M. E., and Kohlstedt, D. L. (1998). High-temperature deformation of dry diabase with application to tectonics on Venus. *Journal of Geophysical Research: Solid Earth*, 103(1):975–984.

Maggi, A., Jackson, J. A., McKenzie, D., and Priestley, K. (2000a). Earthquake focal depths, effective elastic thickness, and the strength of the continental lithosphere. *Geology*, 28(6):495.

Maggi, A., Jackson, J. A., Priestley, K., and Baker, C. (2000b). A re-assessment of focal depth distributions in southern Iran, the Tien Shan and northern India: do earthquakes really occur in the continental mantle? *Geophysical Journal International*, 143(3):629–661.

McGroder, M. F., Lease, R. O., and Pearson, D. M. (2015). Along-strike variation in structural styles and hydrocarbon occurrences, Subandean fold-and-thrust belt and inner foreland, Colombia to Argentina. In DeCelles, P. G., Ducea, M. N., Carrapa, B., and Kapp, P. A., editors, *Geodynamics of a Cordilleran Orogenic System: The Central Andes of Argentina and Northern Chile*. Geological Society of America.

McKenzie, D., Jackson, J., and Priestley, K. (2005). Thermal structure of oceanic and continental lithosphere. *Earth and Planetary Science Letters*, 233(3):337–349.

McKenzie, D., McKenzie, J., and Fairhead, D. (2019). The mechanical structure of Tibet. *Geophysical Journal International*, 217(2):950–969.

McKenzie, D. and Priestley, K. (2016). Speculations on the formation of cratons and cratonic basins. *Earth and Planetary Science Letters*, 435:94–104.

McQuarrie, N. (2002). The kinematic history of the central Andean fold-thrust belt, Bolivia: Implications for building a high plateau. *Bulletin of the Geological Society of America*, 114(8):950–963.

Meigs, A. J. and Nabelek, J. (2010). Crustal-scale pure shear foreland deformation of western Argentina. *Geophysical Research Letters*, 37(11).

Menegon, L., Pennacchioni, G., Malaspina, N., Harris, K., and Wood, E. (2017). Earthquakes as Precursors of Ductile Shear Zones in the Dry and Strong Lower Crust. *Geochemistry, Geophysics, Geosystems*, 18(12):4356–4374.

Mercier, J. L., Sebrier, M., Lavenu, A., Cabrera, J., Bellier, O., Dumont, J.-F., and Machrare, J. (1992). Changes in the tectonic regime above a subduction zone of Andean Type: The Andes of Peru and Bolivia during the Pliocene-Pleistocene. *Journal of Geophysical Research*, 97(B8):11945.

Molnar, P., Chen, W.-P., Fitch, T. J., Tapponnier, P., Warsi, W. E. K., and Wu, F. (1977). Structure and Tectonics of the Himalaya: A brief summary of relevant geophysical observations. In *Collogue Internationaux du CNRS, No. 268, Himalaya: Sciences de la Terre*, pages 269–294, Paris. du Centre National de la Recherche Scientifique.

Molnar, P. and Lyon-Caen, H. (1988). Some simple physical aspects of the support, structure, and evolution of mountain belts. In *Geological Society of America Special Papers*, volume 218, pages 179–208. Geological Society of America.

Molnar, P. and Lyon-Caen, H. (1989). Fault plane solutions of earthquakes and active tectonics of the Tibetan Plateau and its margins. *Geophysical Journal International*, 99(1):123–154.

Mora, A., Parra, M., Strecker, M. R., Kammer, A., Dimaté, C., and Rodríguez, F. (2006). Cenozoic contractional reactivation of Mesozoic extensional structures in the Eastern Cordillera of Colombia. *Tectonics*, 25(2).

Newton, R. C. (1990). Fluids and shear zones in the deep crust. *Tectonophysics*, 182(1-2):21–37.

Nocquet, J. M., Villegas-Lanza, J. C., Chlieh, M., Mothes, P. A., Rolandone, F., Jarrin, P., Cisneros, D., Alvarado, A., Audin, L., Bondoux, F., Martin, X., Font, Y., Régnier, M., Vallée, M., Tran, T., Beauval, C., Maguiña Mendoza, J. M., Martinez, W., Tavera, H., and Yepes, H. (2014). Motion of continental slivers and creeping subduction in the northern Andes. *Nature Geoscience*, 7(4):287–291.

Oncken, O., Hindle, D., Kley, J., Elger, K., Victor, P., and Schemmann, K. (2006). Deformation of the Central Andean Upper Plate System Facts, Fiction, and Constraints for Plateau Models. In *The Andes*, pages 3–27. Springer Berlin Heidelberg.

Poveda, E., Monsalve, G., and Vargas, C. A. (2015). Receiver functions and crustal structure of the northwestern Andean region, Colombia. *Journal of Geophysical Research: Solid Earth*, 120(4):2408–2425.

Priestley, K. and McKenzie, D. (2013). The relationship between shear wave velocity, temperature, attenuation and viscosity in the shallow part of the mantle. *Earth and Planetary Science Letters*, 381:78–91.

Ramos, V. A. (2009). Anatomy and global context of the Andes: Main geologic features and the Andean orogenic cycle. In Kay, S. M., Ramos, V. A., and Dickinson, W. R., editors, *Backbone of the Americas: Shallow subduction, Plateau Uplift ad Terrane Collision*, pages 31–65. Geological Society of America Memoir 204.

Rybacki, E. and Dresen, G. (2004). Deformation mechanism maps for feldspar rocks. *Tectonophysics*, 382(3-4):173–187.

Salfity, J. A. and Marquillas, R. A. (1994). Tectonic and Sedimentary Evolution of the Cretaceous-Eocene Salta Group Basin, Argentina. In Salfity, J. A., editor, *Cretaceous Tectonics of the Andes*, pages 266–315. Vieweg.

Sandiford, M. and Powell, R. (1986). Deep crustal metamorphism during continental extension: modern and ancient examples. *Earth and Planetary Science Letters*, 79(1-2):151–158.

Sempere, T., Carlier, G., Soler, P., Fornari, M., Carlotto, V., Jacay, J., Arispe, O., Néraudeau, D., Cárdenas, J., Rosas, S., and Jiménez, N. (2002). Late Permian-Middle Jurassic lithospheric thinning in Peru and Bolivia, and its bearing on Andean-age tectonics. *Tectonophysics*, 345(1-4):153–181.

Sibson, R. H. (1982). Fault zone models, heat flow, and the depth distribution of earthquakes in the continental crust of the United States. *Bulletin of the Seismological Society of America*, 72(1):151–163.

Sibson, R. H. (1990). Conditions for fault-valve behaviour. *Geological Society Special Publication*, 54(1):15–28.

Sibson, R. H. (1995). Selective fault reactivation during basin inversion: Potential for fluid redistribution through fault-valve action. *Geological Society Special Publication*, 88(88):3–19.

Sloan, R. A., Jackson, J. A., McKenzie, D., and Priestley, K. (2011). Earthquake depth distributions in central Asia, and their relations with lithosphere thickness, shortening and extension. *Geophysical Journal International*, 185(1):1–29.

Smalley, R. and Isacks, B. L. (1990). Seismotectonics of thin- and thick-skinned deformation in the Andean foreland from local network data: evidence for a seismogenic lower crust. *Journal of Geophysical Research*, 95(B8):12487–12498.

Sørensen, B. E., Grant, T., Ryan, E. J., and Larsen, R. B. (2019). In situ evidence of earthquakes near the crust mantle boundary initiated by mantle CO2 fluxing and reaction-driven strain softening. *Earth and Planetary Science Letters*, 524:115713.

Sørensen, K. (1983). Growth and dynamics of the Nordre Stromfjord shear zone. *Journal of Geophysical Research*, 88(B4):3419–3437.

Spikings, R., Reitsma, M. J., Boekhout, F., Mišković, A., Ulianov, A., Chiaradia, M., Gerdes, A., and Schaltegger, U. (2016). Characterisation of Triassic rifting in Peru and implications for the early disassembly of western Pangaea. *Gondwana Research*, 35:124–143.

Starck, D. (2010). Cuenca Cretàcica-Paleógena Del Noroeste Argentino. In *VIII Congreso de Exploración y Desarrollo de Hidrocarburos Simposio Cuencas Argentinas*, pages 407–453, Instituto Argentino del Petróleo y el Gas.

Suárez, G., Gagnepain, J., Cisternas, A., Hatzfeld, D., Molnar, P., Ocola, L., Roecker, S. W., and Viodé, J. P. (1990). Tectonic deformation of the Andes and the configuration of the subducted slab in central Peru; results from a microseismic experiment. *Geophysical Journal International*, 103(1):1–12.

Suarez, G., Molnar, P., and Burchfiel, B. C. (1983). Seismicity, fault plane solutions, depth of faulting, and active tectonics of the Andes of Peru, Ecuador, and southern Colombia. *Journal of Geophysical Research*, 88(B12):10403–10428.

Taymaz, T., Jackson, J. A., and Westaway, R. (1990). Earthquake mechanisms in the Hellenic Trench near Crete. *Geophysical Journal International*, 102(3):695–731.

Turcotte, D. L. and Schubert, G. (2002). *Geodynamics*. Cambridge University Press.

Vaca, S., Vallée, M., Nocquet, J. M., and Alvarado, A. (2019). Active deformation in Ecuador enlightened by a new waveform-based catalog of earthquake focal mechanisms. *Journal of South American Earth Sciences*, 93:449–461.

Watts, A., Lamb, S., Fairhead, J., and Dewey, J. (1995). Lithospheric flexure and bending of the Central Andes. *Earth and Planetary Science Letters*, 134(1-2):9–21.

Weller, O. M., Mottram, C. M., St-Onge, M. R., Möller, C., Strachan, R., Rivers, T., and Copley, A. (2021). The metamorphic and magmatic record of collisional orogens. *Nature Reviews Earth & Environment*, pages 1–19.

Whyte, A. J., Weller, O. M., Copley, A. C., and St-Onge, M. R. (2021). Quantifying water diffusivity and metamorphic reaction rates within mountain belts, and their implications for the rheology of cratons. *Geochemistry Geophysics Geosystems*, n/a(n/a):n/a.

Wimpenny, S., Benavente, C., Copley, A., Garcia, B., Rossell, L., O'Kane, A., and Aguirre, E. (2020). Observations and Dynamical Implications of Active Normal Faulting in South Peru. *Geophysical Journal International*, 222(1):27–53.

Wimpenny, S., Copley, A., Benavente Escobar, C. L., and Aguirre, E. (2018). Extension and Dynamics of the Andes inferred from the 2016 Parina (Huarichancara) Earthquake. *Journal of Geophysical Research: Solid Earth*, 123(9):8198–8228.

Yardley, B. W. D. and Valley, J. W. (1997). The petrologic case for a dry lower crust. *Journal of Geophysical Research*, 102(97):12173–12185.

Zwick, P., McCaffrey, R., and Abers, G. (1994). MT5 Program.

Tables

Location	v_x [mm/yr]	W [km]	$\dot{\varepsilon}^g_{xx}$ [10^{-8} 1/yr]	T_s [km]	$\dot{\varepsilon}^q_{xx}$ [10^{-8} 1/yr]	$\dot{\varepsilon}^q_{xx}/\dot{\varepsilon}^g_{xx}$ [%]
Northern and Southern Andes						
S. Pampeanas	6±1	400±50	1.6±0.4	40	1.50	70–130
C. Peru	3±1	350±50	0.9±0.4	45	0.50	40–100
N. Peru	3±1	350±50	0.9±0.4	40	0.85	65-170
Ecuador	5±1	300±50	1.8±0.8	30	2.70	170-270
Central Andean Plateau						
Bolivia	5±1	200±50	2.8±1.2	40	0.02	0.5-1
S. Peru	4±1	200±50	2.0±1.2	40	0.20	6-25

Table 1: Comparison of geodetic and seismic deformation rates in the Andean forelands. v_x is the range-perpendicular shortening rate inferred from the GPS measurements of Kendrick et al. [2001], Nocquet et al. [2014] and Kendrick et al. [2006], and W is the width of the deforming zone measured perpendicular to the range front. $\dot{\varepsilon}^g_{xx}$ is the average horizontal strain rate perpendicular to the range, and is equivalent to v_x/W. $\dot{\varepsilon}^q_{xx}$ is the range-perpendicular horizontal strain rate inferred from a summation of earthquake moment tensors using a shear modulus of 30 GPa and the seismogenic thickness T_s.

Region	z_{lm} [km]	z_{lf} [km]	z_{cm} [km]	z_{cf} [km]	Δh [km]	F_b [TN/m]
Colombia	150–175	125–150	60–65	30–35	2.7–3.0	3.4±0.4
Ecuador	100–150	125–150	50–60	30–35	2.8–3.0	3.2±0.3
N. Peru	100–150	125–150	50–55	35–40	2.8–3.2	3.7±0.4
C. Peru	100–150	125–175	65–75	35–40	3.8–4.2	5.4±0.6
S. Peru	150–175	125–150	70–75	35–40	4.0–4.3	5.7±0.6
Bolivia	150–200	125–150	70–75	35–40	3.5–3.8	5.1±0.5
Puna	150–175	125–150	70–75	35–40	4.0–4.5	5.9±0.7

Table 2: Parameter range used to calculate the buoyancy force F_b at different points along-strike. z_{lm} = lithosphere thickness beneath the mountains, z_{lf} = lithosphere thickness beneath the forelands, z_{cm} = crustal thickness beneath the mountains, z_{cf} = crustal thickness beneath the forelands, and Δh is the height difference between the mountain range and foreland. The mean of F_b and the 95th percentile range of models are quoted. The fixed parameters are: crustal density = 2800 kg/m^3, mantle density = 3330 kg/m^3, density difference between depleted mantle lithosphere and asthenosphere = -50 kg/m^3, crustal thermal expansivity = 3×10^{-5} W/m/K, Moho temperature beneath the mountains 700–1000 $^\circ C$, and Moho temperature beneath the forelands = 600–700 $^\circ C$.

Figures

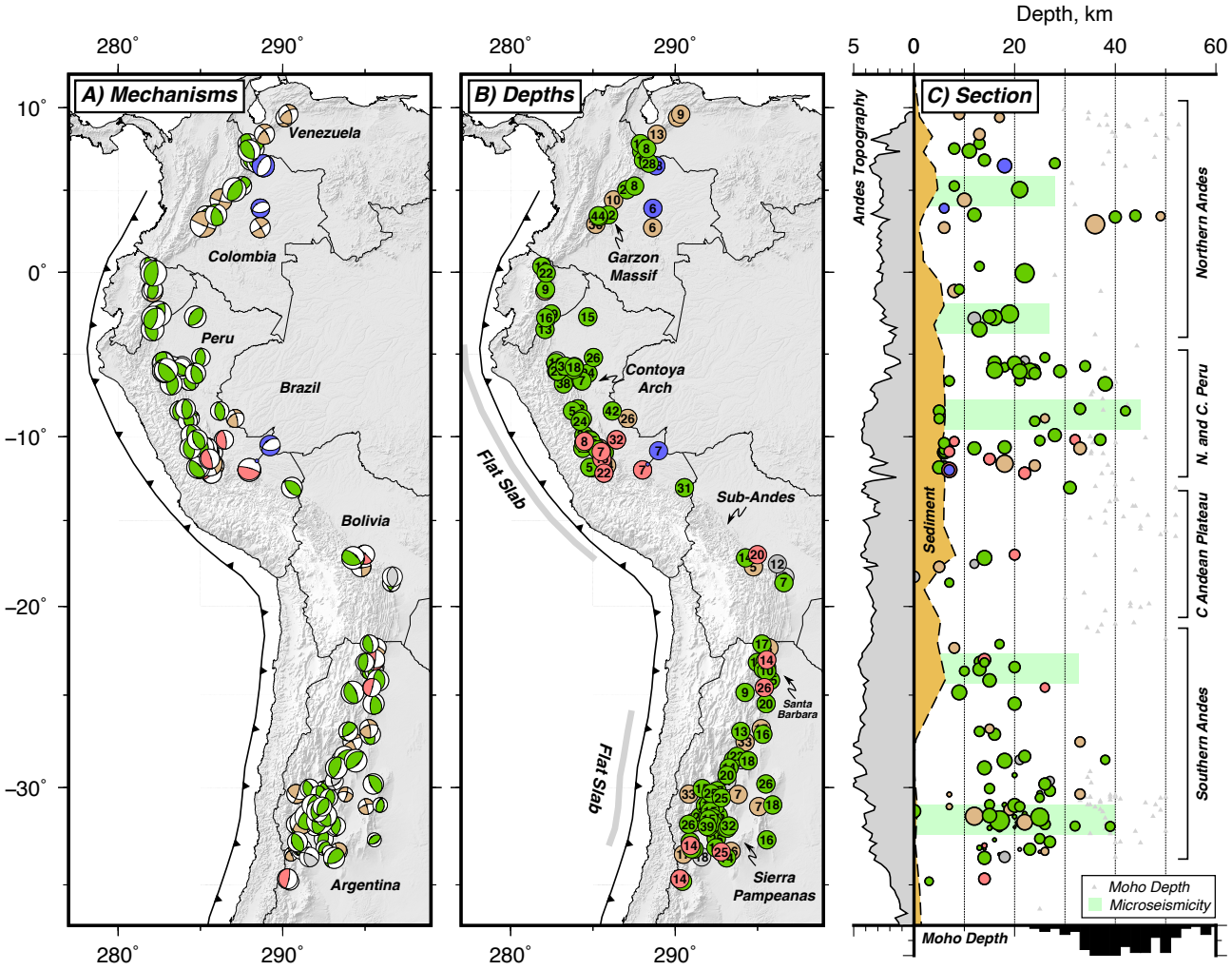

Figure 1: Well-constrained focal mechanisms and centroid depths for earthquakes in the forelands of the Andes. (a) Earthquake mechanisms coloured by the mechanism type, with reverse faults in green, low-angle thrusts in red, normal faults in blue and strike-slip faults in brown. (b) Earthquake centroid depths in kilometres. (c) Section of the centroid depth distribution in the forelands along-strike. Grey circles in (c) are events that do not have a well-constrained focal mechanism. Each circle is scaled in size by the earthquake magnitude. Green bars represent the depth extent of microseismicity from local earthquake and aftershock surveys. The Moho depth variation in the foreland is shown by grey triangles and is taken from receiver function studies [Assumpção et al., 2013; Poveda et al., 2015; Condori et al., 2017]. The sediment thickness in the foreland is taken from Golonka et al. [1995].

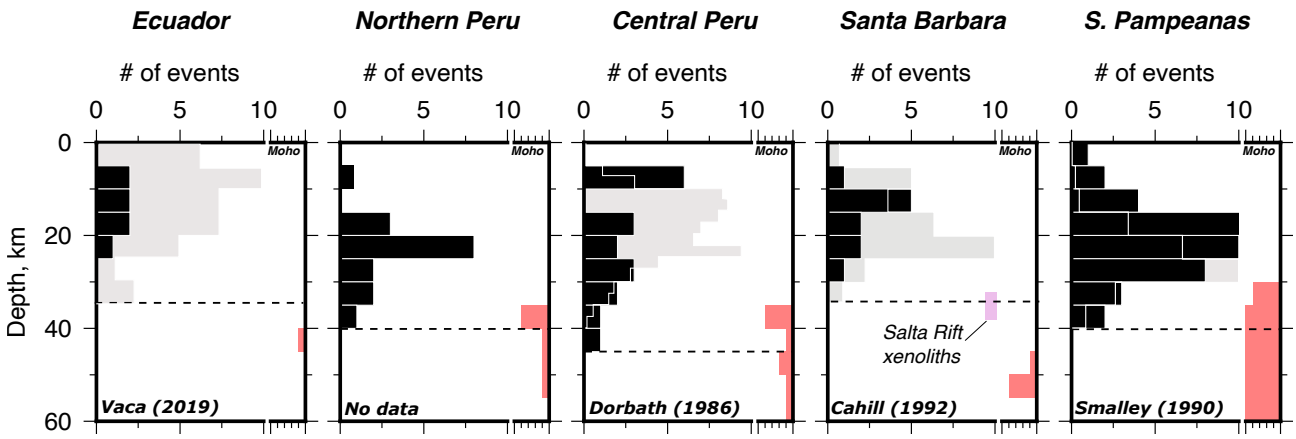

Figure 2: Histograms of the centroid depths of moderate-magnitude earthquakes (black bars), and regional and local microseismicity studies (grey bars with white outline), in different sections of the forelands. The maximum number of microseismic events in each region is normalised to 10 to display the relative distribution with depth. The source of the microseismicity data is shown in the bottom left of each plot. A histogram of the Moho depth in each region is also shown by the red bars on the right of each plot. The horizontal black-dashed line marks the thickness of the seismogenic layer T_s to the nearest 5 km. The depth range of granulite xenoliths erupted from the Salta Rift (discussed in Section 5) are shown by a purple bar.

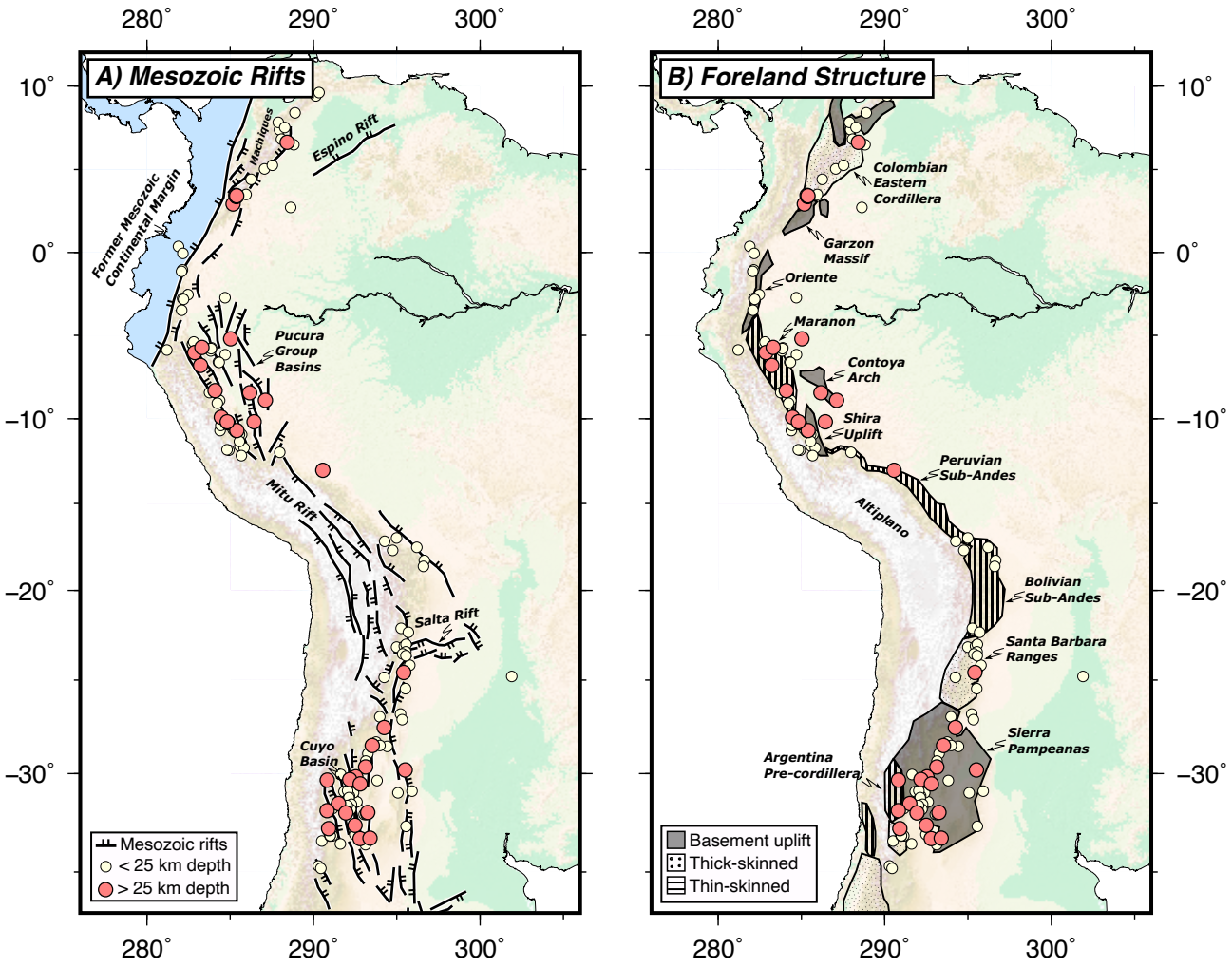

Figure 3: Earthquake distribution compared to the loci of Mesozoic rifts (a) and the structural style of shortening in the Andean forelands (b). The simplified traces of the Mesozoic rifts in (a) are taken from Ramos [2009] and McGroder et al. [2015]. Earthquakes are shown by circles and are coloured light red if they have a centroid depth > 25 km. Rift-related faults running through the Chilean forearc are omitted for clarity. In (b) the along-strike variability in the structural style of foreland deformation is split into three different styles: thin-skinned, thick-skinned and basement uplifts. The deformation style is taken from Kley et al. [1999].

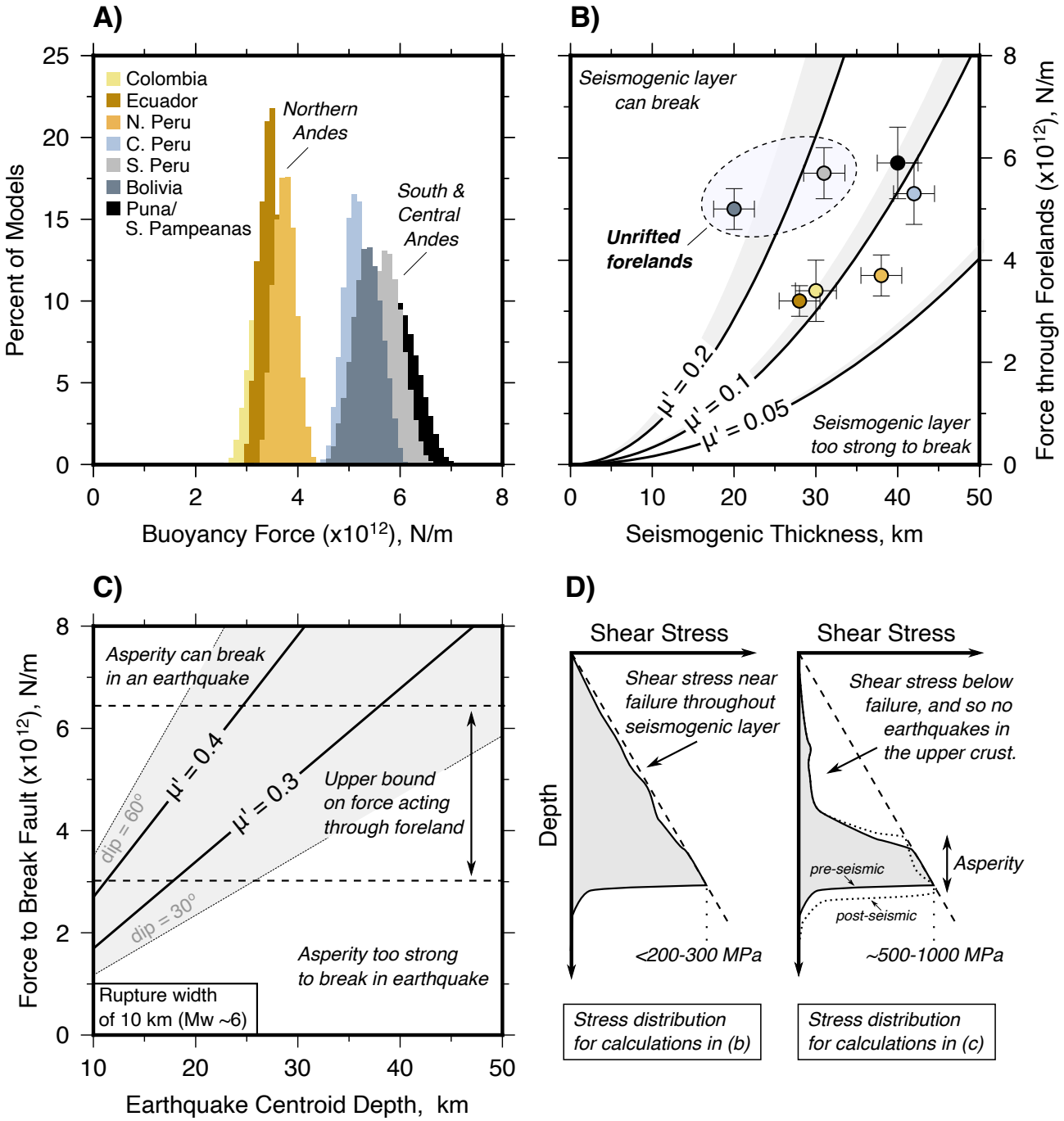

Figure 4: Calculations of the forces acting through the foreland lithosphere and the frictional properties of the foreland faults. (a) Histogram of the buoyancy force F_b acting between the mountains and forelands in seven different regions of the Andes (parameters in Table 2). (b) Seismogenic thickness T_s against the estimate of the force acting through the foreland lithosphere F_f. The uncertainty bars are ± 3 km in T_s and the 95-th percentile of the models in F_f. The thick black lines show the force required to break the seismogenic layer F_{sl} for a given T_s along reverse faults with a 45° dip. Grey-shaded regions show the range of F_{sl} for fault dips between 30° and 60°. (c) Calculation for the force required to break fault asperities in the forelands of the Andes in a $M_w \sim 6$ earthquake at a given centroid depth, assuming a dip of 45° (thick black lines) or 30–60° (grey-shaded region). Horizontal-dashed lines show the force available to break the asperity from (a). (d) Schematic diagram showing the stress distribution with depth along an active fault assumed in the calculations shown in (b) and (c).

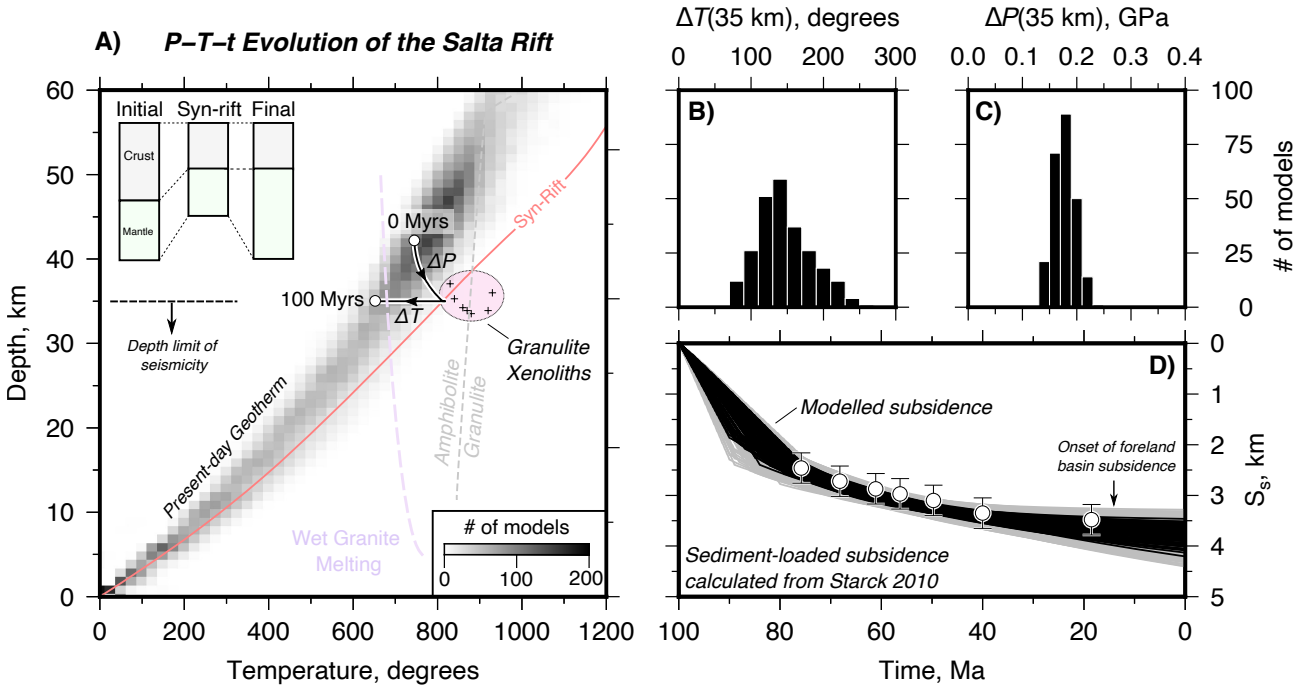

Figure 5: Theoretical estimates of the pressure-temperature-time (P-T-t) evolution for rocks in the lower crust beneath the Salta Rift calculated using thermo-kinematic models that fit the sediment-loaded subsidence history within the Metán-Alemania Basin and the temperature constraints from xenolith thermobarometry. (a) Example P-T-t history for rocks exhumed to 35 km depth (black line) and the associated syn-rift geotherm (light red line) from one particular model. The range of possible present-day geotherms is shown by the density plot in the background, which is calculated from all of the models that match the geological constraints and the observed subsidence history (S_s) to within $\chi^2 < 3$ (see Supplementary Text S2). (b) Distribution of the temperature decrease ΔT for a rock volume exhumed to 35 km depth, and (c) distribution of the equivalent pressure decrease ΔP assuming a crustal density of 2800 kg/m^3. (d) Decompacted sediment-loaded subsidence history (S_s) in the Metán-Alemania Basin from Starck [2010] (white dots) and the model predictions (S_m). Black lines = models that fit to within $\chi^2 < 1$, grey lines = models that fit to within $\chi^2 < 3$.

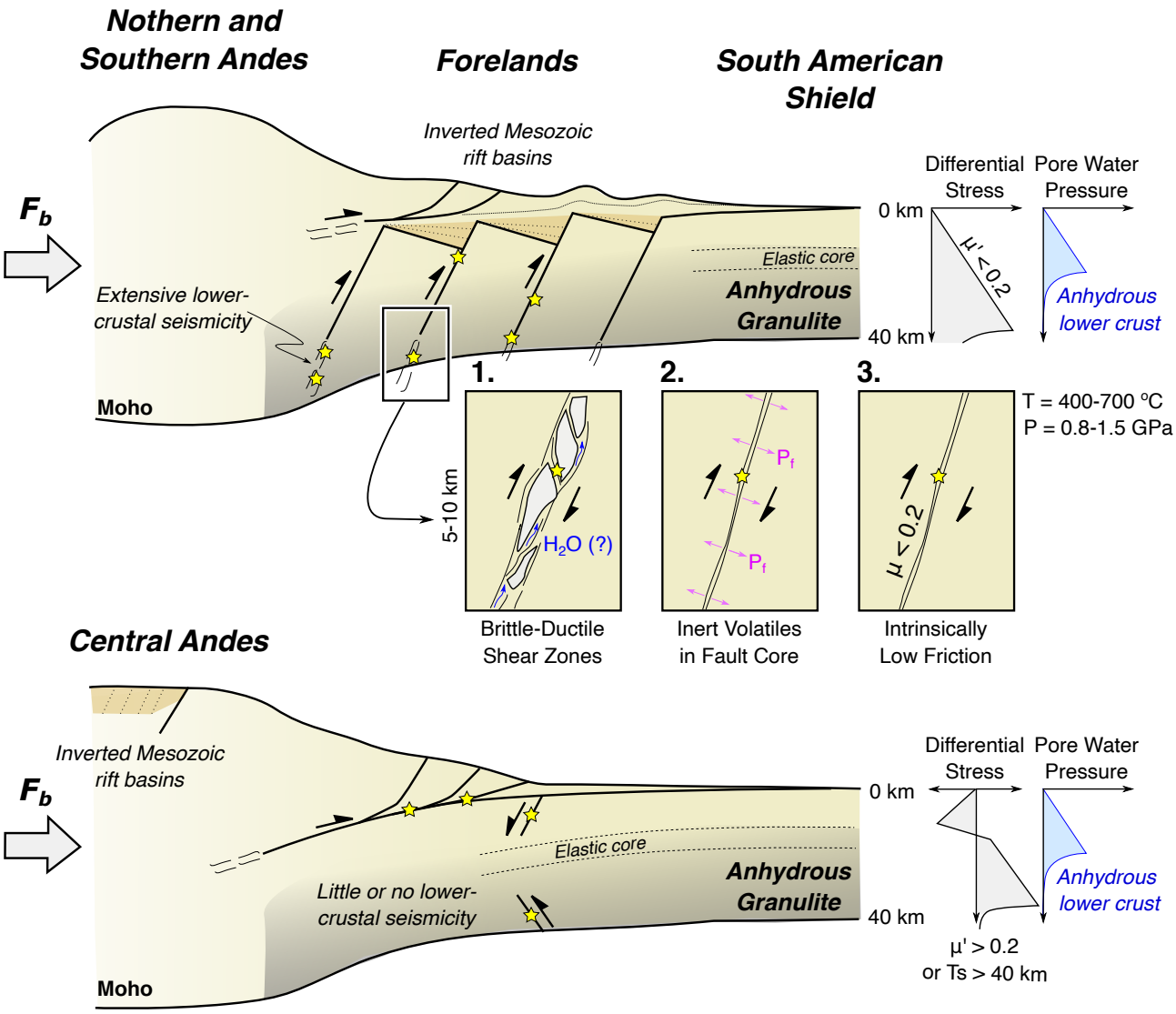

Figure 6: Sketches of the two contrasting styles of shortening in the forelands of the northern and southern Andes (top) and the central Andes (bottom). In the northern and southern Andes, frictionally-weak faults inherited from Mesozoic rift systems that cut through the lower crust are breaking in earthquakes down to ~40–45 km depth. Three different mechanical explanations for how these deep faults may be both seismogenic and frictionally weak are shown, with each of these mechanisms being consistent with the strong, dry lower crust beneath the Andean forelands. Along the margins of the central Andean plateau, there has been little or no recent seismicity in the lower crust, and the foreland is thought to underthrusting the high plateau. In this area the Mesozoic rift basins can be identified within the interior of the mountain range. The top of the foreland crust is in extension and its base is in compression, suggesting the seismogenic layer is bending beneath the mountains.